# THERMOCLINE WATER TEMPERATURE GRADIENT AT THE INDONESIAN THROUGHFLOW PATHWAYS DURING LAST GLACIAL MAXIMUM (LGM)

# *GRADIEN TERMOKLIN TEMPERATUR LAUT PADA JALUR ARUS LINTAS INDONESIA SAAT GLASIAL MAKSIMUM TERAKHIR*

**Rima Rachmayani[1*], Oktavira Dwi Demia Larasati[2], Marfasran Hendrizan[3]**

[1] Research Group of Environmental and Applied Oceanography, Faculty of Earth Sciences and Technology, Bandung Institute of Technology, Indonesia

[2] Study Program of Earth Science, Faculty of Earth Sciences and Technology, Bandung Institute of Technology, Indonesia

[3] Paleoclimate and Paleoenvironment Research Group, National Research and Innovation Agency (BRIN), Indonesia

*Corresponding author: rrachmayani@itb.ac.id

(Received 08 April 2025; in revised from 10 April 2025; accepted 05 June 2025)

DOI : 10.32693/bomg.40.1.2025.937

**ABSTRACT**: This study aims to investigate the strength of the Indonesian Throughflow (ITF) during the Last Glacial Maximum (LGM) in comparison to the Pre-Industrial (PI) at the Makassar Strait, the Molucca Sea, and the Banda Sea, representing the pathways of the ITF. The analysis was performed based on the temperature distribution of the south (S) and north (N) thermocline gradients. Temperature data were obtained from the simulation of the Climate Community System Model, version 4 (CCSM4). The depth of the thermocline layer during the LGM and the PI period exhibits seasonal variability across the S-N stations. At Station 1, 2, and 3, the thermocline depth during the LGM ranges from 49 - 218 m (51 - 251 m), 55 - 250 m (69 - 254 m), and 48 - 238 m (48 - 218 m) in the south (north), respectively. The analysis of seasonal temperature variations in the thermocline layer in the three locations indicates that the ITF was significantly weakened both during the LGM and PI, indicated by the negative S-N Thermocline Water Temperature (TWT) gradient. The result suggests the southern part of each station is predominantly fresher compared to the northern part during these times. Additionally, it implies that the ITF is more robust in the eastern region (Banda Sea) during the LGM compared to the PI. This variation may relate to the intensity of seasonal local winds, mixing processes, and the remote influence of El Niño-like events, which could affect water transport along the pathway of the ITF.

**Keywords**: Thermocline Water Temperature, Indonesian Throughflow, Last Glacial Maximum, Makassar Strait, Molucca Sea, Banda Sea

***ABSTRAK***: *Penelitian ini bertujuan untuk menyelidiki kekuatan Arus Lintas Indonesia (Arlindo) selama Last Glacial Maximum (LGM) dibandingkan dengan Pra-Industri (PI) di Selat Makassar, Laut Maluku, dan Laut Banda, yang mewakili jalur Arlindo. Analisis dilakukan berdasarkan distribusi gradien suhu pada lapisan termoklin di stasiun bagian selatan (S) dan utara (N). Data suhu diperoleh dari simulasi Climate Community System Model, version 4 (CCSM4). Kedalaman lapisan termoklin selama LGM dan periode PI menunjukkan variabilitas musiman di seluruh stasiun S-N. Di Stasiun 1, 2, dan 3, kedalaman termoklin selama LGM berkisar antara 49 - 218 m (51 - 251 m), 55 - 250 m (69 - 254 m), dan 48 - 238 m (48 - 218 m) di selatan (utara), secara berurutan. Analisis variasi suhu musiman pada lapisan termoklin di tiga lokasi menunjukkan bahwa ITF melemah secara signifikan baik selama LGM maupun PI, ditunjukkan oleh gradien Thermocline Water Temperature (TWT) di stasiun S-N yang negatif. Hasil ini menunjukkan bahwa bagian selatan setiap stasiun menyimpan air tawar lebih banyak dibandingkan dengan bagian*

*utara pada LGM dan PI. Selain itu, hal ini menyiratkan bahwa ITF lebih kuat di wilayah timur (Laut Banda) selama LGM dibandingkan dengan PI. Variasi ini mungkin berhubungan dengan intensitas angin lokal musiman, proses pencampuran, dan pengaruh dari El Niño-like, yang dapat mempengaruhi transpor massa air di sepanjang jalur ITF.*

***Kata Kunci:*** Thermocline Water Temperature, Arus Lintas Indonesia, Last Glacial Maximum, Selat Makassar, Laut Maluku, Laut Banda

# INTRODUCTION

A key component of the Indonesian Throughflow (ITF), which moves warm water from the Pacific to the Indian Ocean, the thermocline is defined by a fast drop in temperature with depth (Gordon, 2005). Thermohaline circulation allows this mechanism to greatly affect world climate patterns (Gordon, 2005; Talley, 2013). Understanding the function of the thermocline in climate dynamics requires study of its temperature gradient over past, present, and future changes within the ITF. The thermocline temperature gradient between the northern and southern part of Makassar Strait, a key route for the ITF, has shown significant variation over the last 30,000 years. Moreover, it showed that the thermocline gradient was more pronounced between 13.4–19 kiloyears ago (ka) and 24.2–27 ka before present (BP) relative to the Holocene epoch at roughly 10 ka BP (Fan et al., 2018). El Niño-like climate conditions cause the ITF to weaken, which lowers trade wind stress. The thermocline inside the ITF is still influenced by monsoonal cycles and tidal mixing. Intensified water mixing in the austral winter produces a thicker mixed layer and more bottom stratification. The future thermocline temperature gradient of the ITF is expected to respond to climate change and associated oceanographic activities.

Studies (e.g., Holbourn et al., 2011; Feng et al., 2017; Zhang et al., 2024) show that changes in the Earth's orbit have affected the upper water layers of the ITF during the past 120,000 years, suggesting that upcoming orbital changes might also affect the thermocline configuration. Future changes are anticipated to come from a mix of human-induced climate change and natural oceanographic processes, hence stressing the need for ongoing monitoring and research to forecast and understand these changes.

A major geological era is the Last Glacial Maximum (LGM). The LGM is known as a time marked by worldwide cooling and a remarkable drop in sea levels. Relative to modern conditions, a sea level drop of up to 120 m (Peltier et al., 2006) exposed the Sunda Shelf, Gulf of Thailand, South China Sea, Java Sea, and Sahul Shelf during this time. El Niño-like circumstances affected the hydroclimatology of the Indonesian waters and the Pacific Ocean during the LGM (Ding et al., 2013; Fan et al., 2018; Pang et al., 2021). Climate conditions turned drier during the LGM, marked by lower atmospheric water content and rainfall, which raised surface salinity in the Indonesian waters (Xu et al., 2008; Linsley et al., 2010). Thus, the ITF showed less strength during the LGM era (Holbourn et al., 2011; Ding et al., 2013; Fan et al., 2018).

Every second, the IFT moves roughly 15 Sv (1 Sv = $10^6$ m³/s) of water mass to the Indian Ocean (Sprintall et al., 2009; Gordon et al., 2010). Contributing about 12–13 Sv, the Makassar Strait is the ITF's primary transport path, accounting for 77% of the total (Gordon et al., 2010). The ITF affects the distribution of heat and salinity in the Pacific and Indian Oceans (Lee et al., 2015; Hu et al., 2019), therefore influencing temperature and precipitation patterns in nearby marine and terrestrial habitats. This has spurred a lot of study meant to grasp the historical development of the ITF. Numerous research investigations have been undertaken to analyse the evolution of ITF in the past using paleoceanographic reconstruction (Bradley, 1999; Holbourn et al., 2011; Ding et al., 2013; Hendrizan et al., 2017; Fan et al., 2018; Pang et al., 2021). However, knowledge of the ITF's evolution in the Makassar Strait and other ITF's pathways is somewhat limited.

The connection between the ITF and the thermocline has not been much studied using numerical modeling. Shen et al., 2023 discussed the ITF and thermocline variability associated with the El Niño-Southern Oscillation (ENSO) and the Indian Ocean Dipole (IOD) by using CMIP5 models. It showed a decline in ITF transport under global warming conditions by 2100 (Shen et al., 2023). Back to the past, Rachmayani et al., (2019) used the Community Climate System Model, version 3 – Dynamic Global Vegetation Model (CCSM3-DGVM), to investigate climatic variability during important Marine Isotope Stages (MIS), revealing seasonal temperature anomalies linked to local insolation. Zuyi (2003) studied the numerical

experiments where the closing of the ITF has caused notable changes in oceanic circulation, hence affecting temperature distributions in the tropical Pacific and Indian Oceans. Though numerical experiments have difficulties related to the complexity of regional climate systems and the limits of historical data, these models provide notable insights.

This study looks at the seasonal temperature distribution at certain ITF pathways, namely the Makassar Strait, Molucca Sea, and Banda Sea, from model output of CCSM4. By looking at temperature layer changes represented by thermocline water temperature gradient (TWT), this study highlights the strength of the ITF during the LGM in relation to PI conditions at the three mentioned locations.

# METHODS

### Study area

Figure 1 displays the area of interest, Indonesia, with three stations selected in the Makassar Strait (Station 1), the Molucca Sea (Station 2), and the Banda Sea (Station 3). The three stations are denoted with red dots in the north (N) and south (S) of each station. This is made to represent ITF pathways.

### Data

Data was manageably taken from the World Data Center for Climate (WDCC). The WDCC is hosted by the German Climate Computing Center (Deutsches Klimarechenzentrum - DKRZ) in Hamburg, and it was openly accessed from https://www.wdc-climate.de/ui/. Since the past and recent climates are considered to be different, one time slice of the LGM at 21,000 years ago is selected to represent the period of glaciation, and the LGM climate is compared to the recent climate represented by PI as a reference. Investigation on TWT in this recent study is carried out by using the CCSM4 both in the LGM and PI model outputs (Brady et al., 2013) under the Paleoclimate Modelling Intercomparison Project, phase 3 (PMIP3) contribution to the Coupled Model Intercomparison Project, phase 5 (CMIP5), PMIP3-CMIP5 LGM experiments (Kageyama et al., 2021). Boundary conditions and forcings are summarised in Table 1.

### Model

The CCSM4 is a general circulation model that integrates components for the atmosphere, ocean,

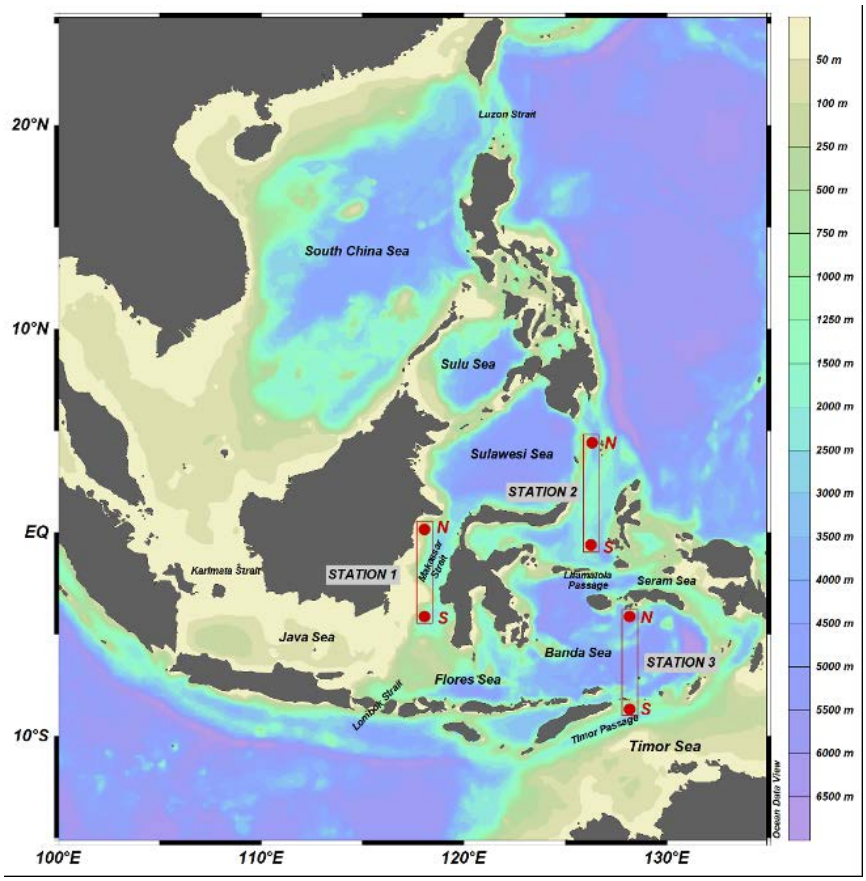


Figure 1. Study area of Indonesia. Shaded colours depict bathymetry; red dots exhibit N-S stations at the selected ITF pathways of Makassar Strait, Molucca Sea, and Banda Sea.

Tabel 1. Boundary conditions and forcings simulated by using CCSM4 (Brady et al., 2013) for LGM and PI experiments

| Simulation | GHGs | Ice sheets | Orbital year | Vegetation/ aerosols | Length of simulation |
|---|---|---|---|---|---|
| PI | $CO_2$ = 284.7 ppm<br>$CH_4$ = 791.6 ppb<br>$N_2O$ = 275.68 ppb | Modern Greenland and Antarctica | 1990 CE | Pre-Industrial | 1,300 yr |
| LGM | $CO_2$ = 185 ppm<br>$CH_4$ = 350 ppb<br>$N_2O$ = 200 ppb | PMIP3 LGM | 21 ka | PI | 1,000 yr |

*Note:*
CE= common era
ka= kilo- annum
yr= year
ppm= part per million
ppb= part per billion

land, and sea ice, exchanging information through a coupler which released in April 2010. Its atmospheric component, CAM4, features a 1.25° × 0.9° resolution with 26 vertical layers, improving El - Niño Southern Oscillation (ENSO) representation and high-latitude stability in LGM simulations. The land model, CLM4, shares the same resolution (Lawrance et al*.,* 2012), incorporating enhanced hydrology and a carbon–nitrogen biogeochemistry model, influencing vegetation responses to climate change. The ocean component (Smith et al*.,* 2010), based on the Parallel Ocean Program (POP2), utilizes a displaced grid with improved Gulf Stream dynamics and reduced sea surface temperature biases. It employs a standard displaced grid with poles positioned in Greenland and Antarctica and features 60 vertical levels (Danabasoglu et al., 2012a). The nominal 1° horizontal resolution consists of a uniform 1.1° spacing in longitude, while latitude varies from 0.27° at the equator to 0.54° at 33° latitude. The sea ice model, derived from the Community Ice Code (CICE4), enhances surface albedo and radiative transfer, leading to better Arctic Sea ice simulations (Hunke and Lipscomb, 2010; Holland et al., 2012) and operates on the same horizontal grid as the ocean component. Overall, CCSM4 introduces key improvements over previous versions, enhancing climate simulation accuracy (Brady et al*.,* 2019). Details on its development and documentation of the 1850 Common Era (CE) PI control simulation can be found in Gent et al. (2011). A wide range of additional simulations has been conducted with CCSM4 as part of CMIP5, including the Last Millennium (Landrum et al*.*, 2012) and future scenario simulations (Meehl et al*.*, 2012).

The LGM simulation, however, implements a more scale-selective fourth-order divergence damping to enhance high-latitude stability in CAM4 by mitigating grid-scale noise caused by steep ice sheets over North America and Greenland (Lauritzen et al*.,* 2012). CAM4 offers notable improvements, including a significantly better representation of the spatial and temporal characteristics of ENSO (Richter and Rasch, 2008; Neale et al., 2008; Deser et al*.,* 2012). For the climate change simulations in this study, while the plant functional type distribution remains fixed at preindustrial values (Lawrence and Chase, 2007), the leaf area index and vegetation height are prognostic and responsive to climate variations (Thornton et al., 2007). A newly implemented overflow parameterisation enhances the Gulf Stream's path and the meridional overturning circulation in the North Atlantic, leading to improved sea surface temperature and salinity accuracy compared to CCSM3 (Danabasoglu et al*.,* 2012b). The increased vertical resolution, especially in the upper ocean, helps mitigate sea surface temperature errors in major upwelling regions and refines the mean and annual cycle of sea surface temperature in the eastern Pacific along the equator (Gent et al*.,* 2011).

# RESULTS

### Seasonal Thermocline Changes During LGM and PI

Figure 2 shows sea temperature vertically from the surface to the deep layer at each N-S station to see the seasonal thermocline occurrences during the LGM. Figure 2a-b exhibits the seasonal thermocline

depth during LGM at Station 1 in the north (N) point at an average depth of 51-254 m and the south (S) point at an average depth of 49-218 m. Figure 2c-d illustrates the thermocline at Station 2 in the north (N) with an average depth of 69-254 m and south (S) points with an average depth of 55-250 m. Figure 2e-f presents the thermocline at Station 3 in the north (N) point with an average depth of 48-218 m and the south (S) point with an average depth of 48 -238 m. Judging from the results, the upper-to-lower seasonal thermocline depth at the three stations experiences slight seasonal changes from 21 to 36 m. Sea surface temperature (SST) at the three stations exhibits a slightly warmer temperature at the north points compared to the south points. Station 1 at Makassar Strait and Station 2 at Molucca Sea experience a similar range of SST of 25.5-27.5°C; meanwhile, Station 3 at Banda Sea experiences a colder SST in a range of 24.5-27.5°C. Seasonal SST changes are clearly seen at every south-north station where the coldest SST in the December-January-February (DJF) season represented by the month of February, is captured at the north stations of Makassar and the Molucca Sea, and the warmest SST is captured during September-October-November (SON) in November, as at every station in the south. Meanwhile, the coldest SST at the south stations occurs five months after February, that is, in July-August (June-July-August, JJA season). Furthermore, sea temperature during the LGM is captured as colder at the surface by 3-5°C and vertically in the thermocline until the deep layer by 2°C compared to the PI at every south-north station. However, the seasonal sea temperature pattern of the thermocline during PI at the three stations looks similar relative to the seasonal sea temperature pattern during LGM.

The thermocline layer depth during LGM and PI (Figure 3) seems similar to each, but varies at south (north) points, where the seasonal thermocline layer during LGM at Station 1 ranges from 36 to 211 m (43 to 224 m), and Station 2 ranges from 42 to 216 m and 53 to 226 m at the south and north stations, respectively. The seasonal thermocline layer at Station 3 ranges at the south (north) from 42 to 178 m (34 to 185 m). It is shown from Figure 2 and Figure 3 that the seasonal changes of the thermocline layer's depth are minor since the seasonal SST changes only occur in the mixed layer depth (MLD). The averaged seasonal thermocline depth at the three stations during LGM and PI is listed in Table 2.

Tabel 2. The averaged seasonal depth of thermocline at the three stations of Makassar Strait, Molucca Sea, and Banda Sea

| No. | Location | Station | Upper Thermocline Depth (m) | | Lower Thermocline Depth (m) | | Maximum and Minimum Temperature at the Thermocline Layer (C) | |
|---|---|---|---|---|---|---|---|---|
| | | | LGM | PI | LGM | PI | LGM | PI |
| 1 | Makassar Strait | North | 51 | 43 | 254 | 224 | 26.89-10.18 | 29.17-13.24 |
| | | South | 49 | 36 | 218 | 211 | 26.28-11.34 | 28.94-13.01 |
| 2 | Molucca Sea | North | 69 | 53 | 254 | 226 | 26.48-10.25 | 29.53-12.18 |
| | | South | 55 | 42 | 250 | 216 | 26.80-10.44 | 29.38-13.05 |
| 3 | Banda Sea | North | 48 | 34 | 218 | 185 | 27.62-12.06 | 29.19-13.10 |
| | | South | 48 | 42 | 238 | 178 | 26.02-10.61 | 29.41-13.38 |

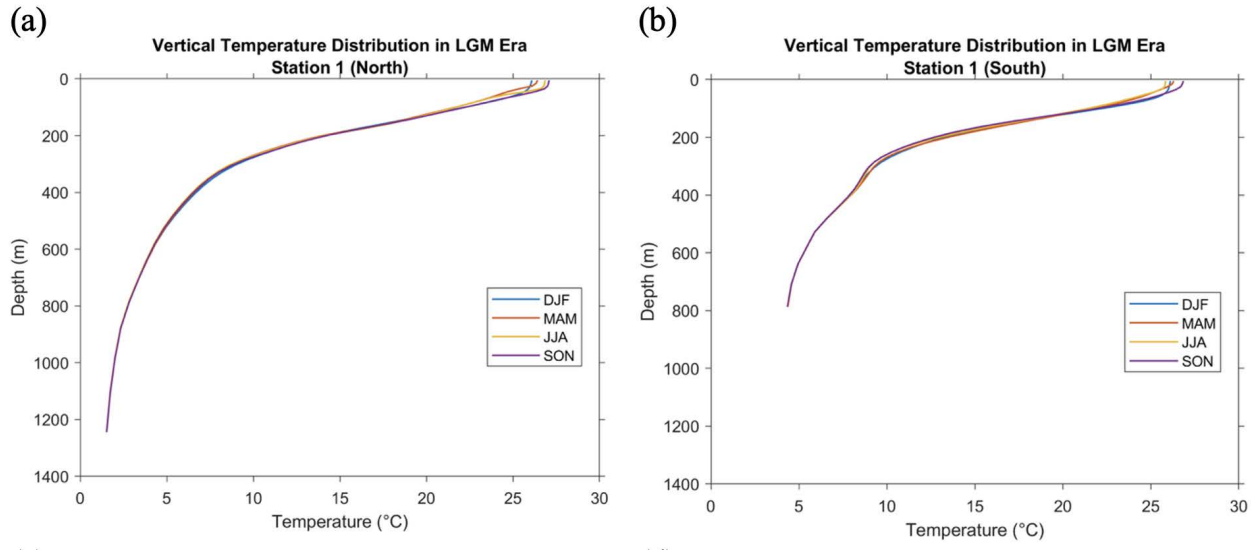

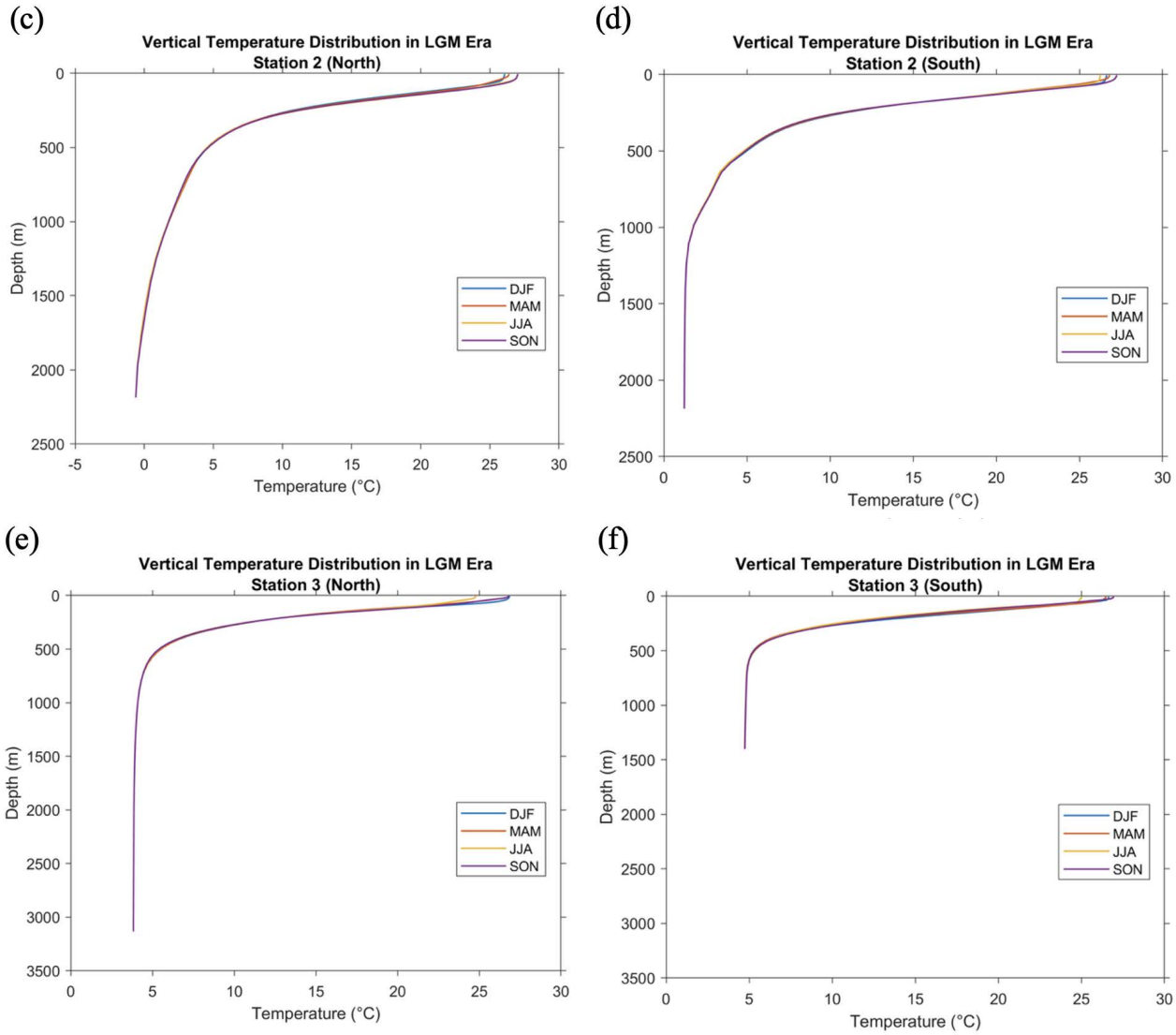


Figure 1. Seasonal vertical sea temperature at the three vertical stations: (a) 1-north, (b) 1-south, (c) 2-north, (d) 2-south, (e) 3-north, and (f) 3-south (see map in Figure 1). Coloured lines show the vertical sea temperature in December-January-February (DJF), March-April-May (MAM), June-July-August (JJA), and September-October-November (SON) during the LGM.

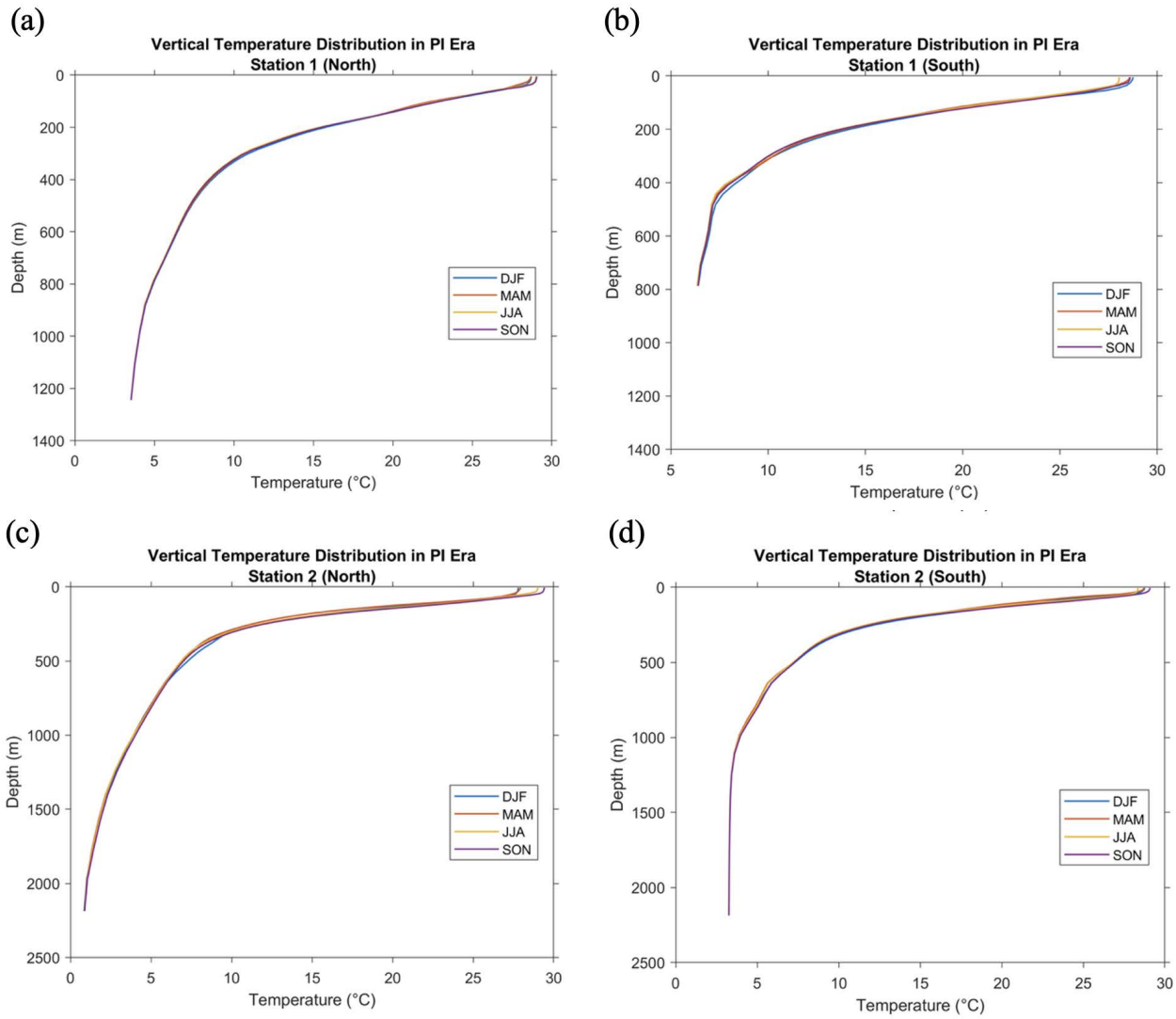


Figure 3. As in Figure 2, but for PI.

**Seasonal Thermocline Water Temperature (TWT) Gradient during LGM and PI**

Figure 4 addresses a gradient of TWT vertically from the surface to the thermocline layer at each S-N station (Table 2) to see the seasonal TWT occurrences during the LGM. Figures 4a-c exhibit the gradient of TWT at stations 1-3 between the south (S) and the north (N) points as listed in Table 2 with maximum depths at each station (Station 1=800 m, Station 2=2,250 m, Station 3=1,500 m). It can be seen that the vertical profile of the S-N TWT gradient at Station 1 (Makassar Strait), Station 2 (Molucca Sea), and Station 3 (Banda Sea) varies, where the negative S-N TWT gradient robustly is captured at 75-254 m depth down to -2.05 °C/m, 45-267 m depth down to -1.63 °C/m, and varies shallower from 25-251 m depth down to -1.25 °C/m at each mentioned station, respectively. While the positive S-N TWT gradient is apprehended lower than 105 m depth at Station 1 (Makassar Strait) up to 0.5 °C/m. Moreover, the positive S-N TWT gradient is captured robustly at 55-251 m depth up to 0.66 °C/m at Station 2 (Molucca Sea), at 25-251m up to 1.45 °C/m at Station 3 (Banda Sea). Additionally, seasonal changes of the S-N TWT gradient are clearly seen at each station. The most negative TWT gradient is exhibited during SON in September and October at 165 m depth, and the most positive TWT gradient is revealed during MAM in March at 85 m depth at Station 1 (Makassar Strait). Meanwhile, at Station 2 (Molucca Sea), the most negative TWT gradient is shown during JJA in July at 115 m depth, and the most positive TWT gradient is experienced during DJF in January at 65 m depth. At Station 3 (Banda Sea), the seasonal changes are similar to Station 1 (Makassar Strait), where the most negative TWT gradient is in September (SON) at 115 m depth, and the most

positive TWT gradient is demonstrated in February (DJF) at 155 m depth.

The S-N TWT gradient during LGM (Figure 4) is compared to the S-N TWT gradient in PI (Figure 5). It is revealed that the seasonal negative S-N TWT gradient vertically shifted and became shallower from 75-254 m depth during the LGM to 25-236 m depth during PI (Station 1, Makassar Strait). At station 2 (Molucca Strait), the negative S-N TWT gradient experienced at depths of 35-251 m during the PI shows a shallower depth at about 10 m compared to the LGM. The positive-to-negative shifted S-N TWT gradient at Station 3 (Banda Sea) occurs clearly at 25-222 m depth during the DJF in LGM compared to PI. Particularly, the TWT gradient during LGM and PI at the thermocline layer (Table 2), is displayed in Table 3.

Tabel 3. Seasonal averages of TWT gradient at the three stations of Makassar Strait, Molucca Sea, and Banda Sea during LGM and PI

| No. | Location | Maximum Thermocline Depth at S-N Stations (m) | | Seasonal | Seasonal averaged TWT gradient (°C/m) | |
|---|---|---|---|---|---|---|
| | | LGM | PI | | LGM | PI |
| 1 | Makassar Strait | 49-254 | 36-224 | DJF | -0.48 | -1.07 |
| | | | | MAM | -0.29 | -1.19 |
| | | | | JJA | -0.82 | -1.39 |
| | | | | SON | -0.94 | -1.14 |
| 2 | Molucca Sea | 55-254 | 42-226 | DJF | 0.15 | -0.38 |
| | | | | MAM | -0.36 | -0.58 |
| | | | | JJA | -1.08 | -1.08 |
| | | | | SON | -0.77 | -0.93 |
| 3 | Banda Sea | 48-238 | 34-185 | DJF | 0.49 | -0.88 |
| | | | | MAM | 0.70 | 0.31 |
| | | | | JJA | -0.32 | 0.19 |
| | | | | SON | -0.35 | -0.74 |

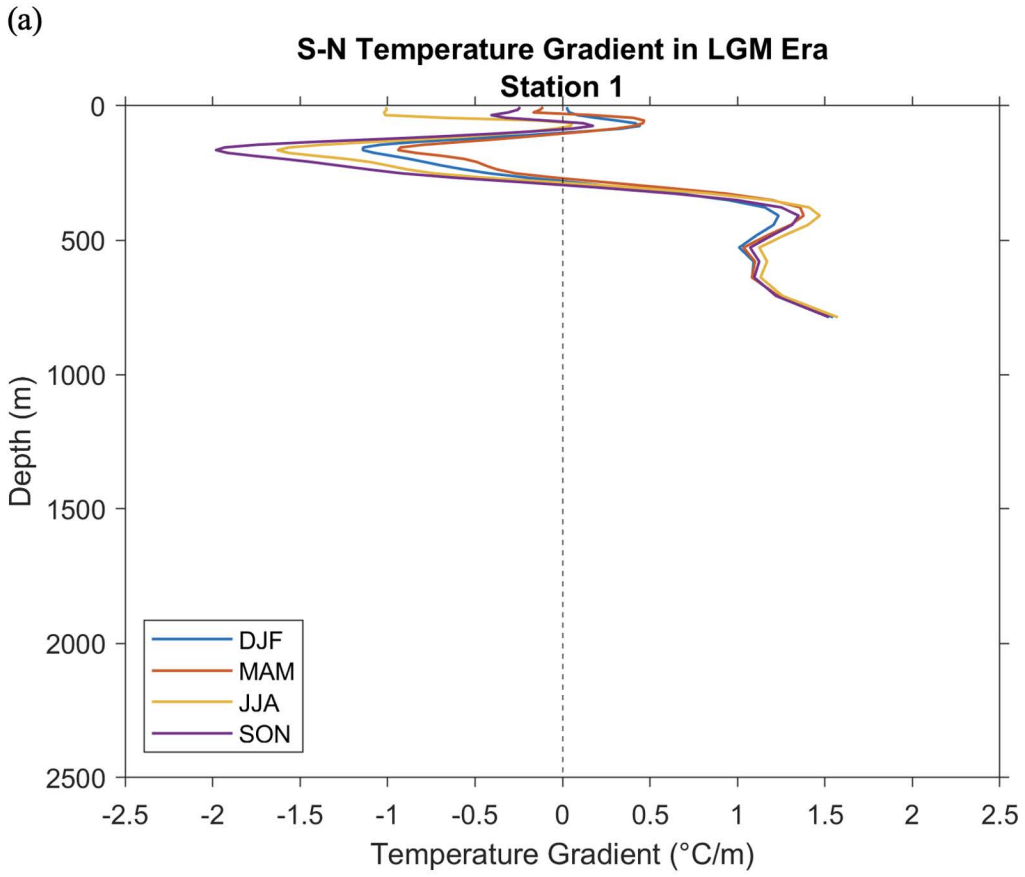

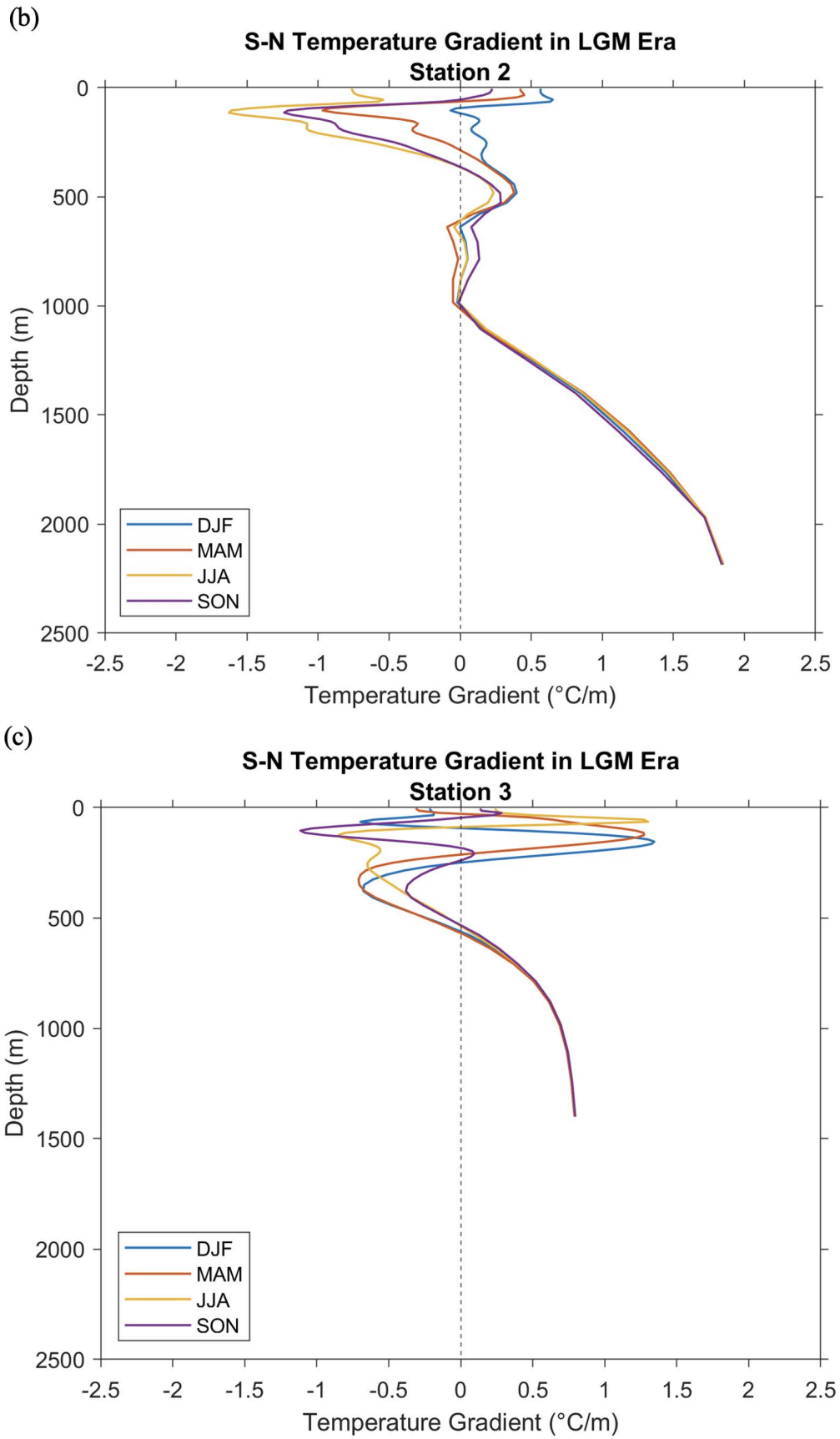


Figure 4. South-North (S-N) thermocline water temperature (TWT) gradient at the three vertical transects: (a) 1, (b) 2, (c) 3 (see map in Figure 1). Coloured lines show the gradient in December-January-February (DJF), March-April-May (MAM), June-July-August (JJA), and September-October-November (SON) during LGM.

(a)

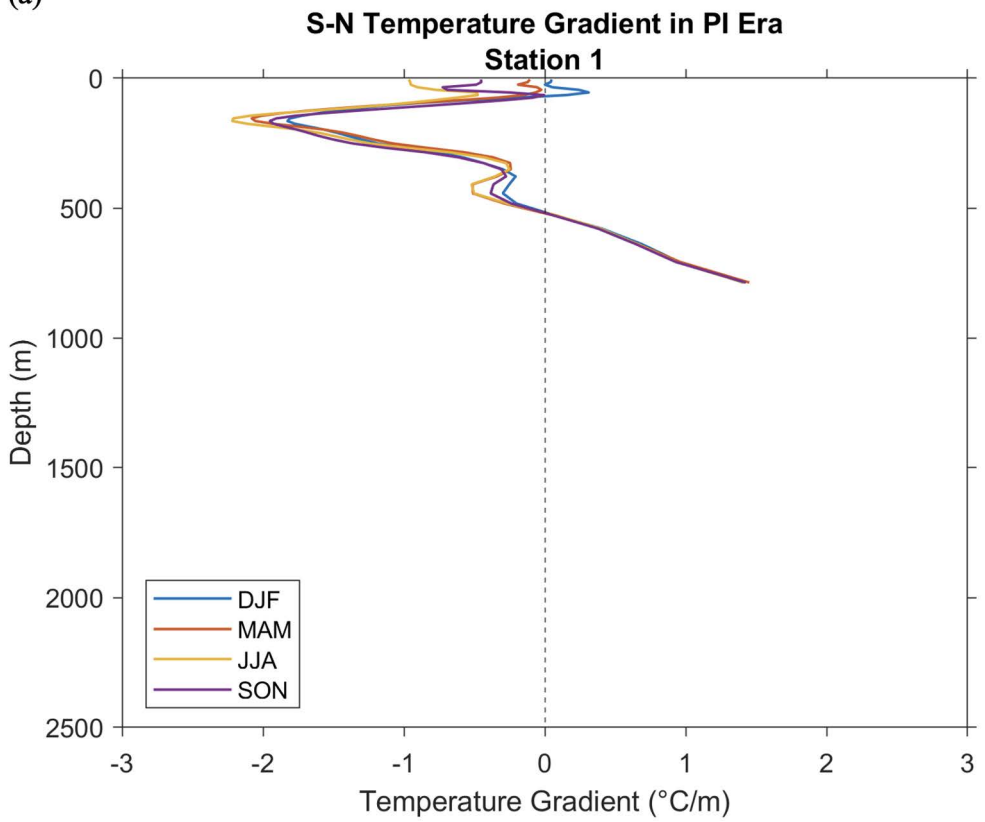
S-N Temperature Gradient in PI Era
Station 1
Depth (m)
0
500
1000
1500
2000
2500
-3
-2
-1
0
1
2
3
Temperature Gradient (°C/m)
DJF
MAM
JJA
SON

(b)

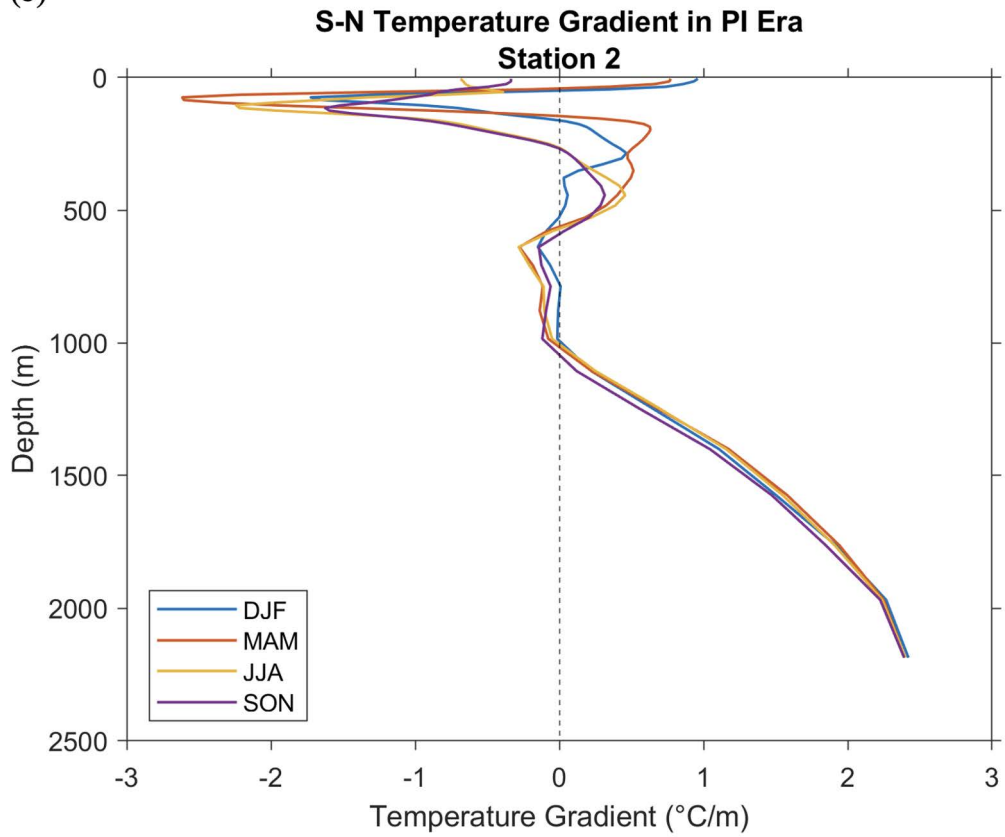
S-N Temperature Gradient in PI Era
Station 2
Depth (m)
0
500
1000
1500
2000
2500
-3
-2
-1
0
1
2
3
Temperature Gradient (°C/m)
DJF
MAM
JJA
SON

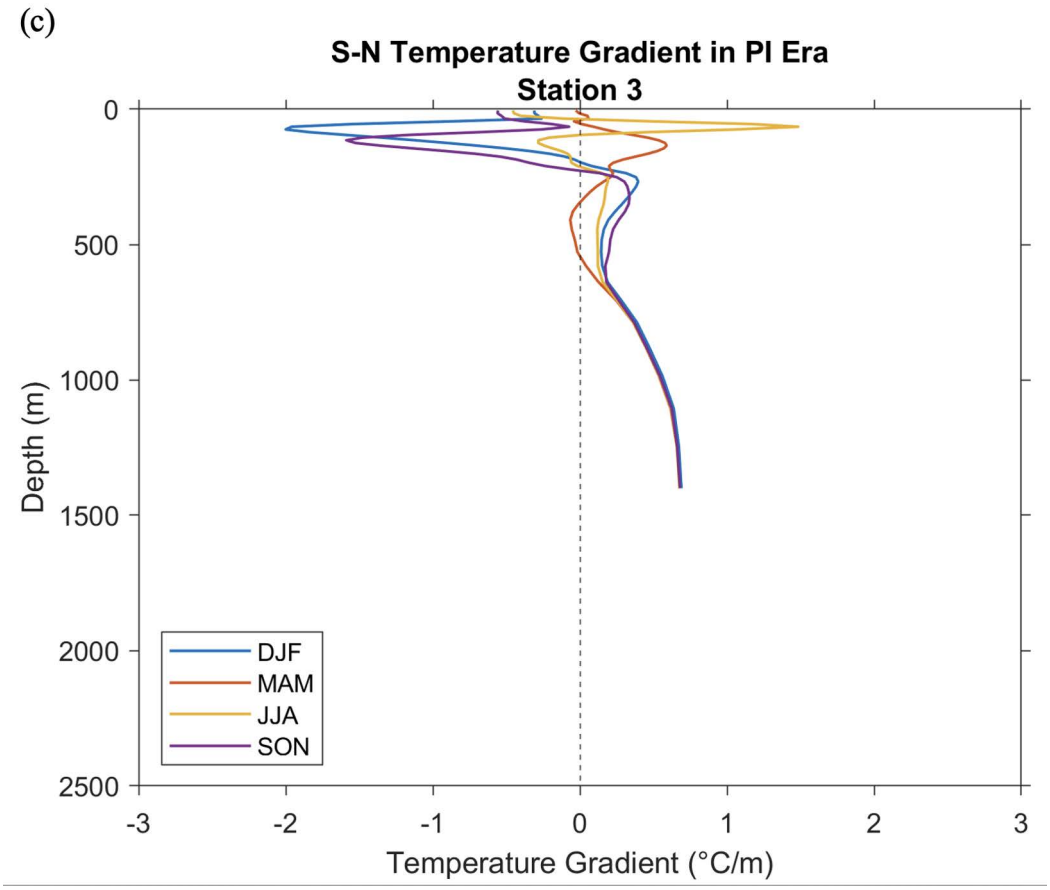


Figure 5. As in Figure 4, but for PI.

## DISCUSSIONS

In equatorial regions, the thermocline develops due to solar radiation and heat transfer, resulting in a significant temperature gradient that limits further changes in heat movement. The ITF's significant role in global heat redistribution has led to extensive research on its historical variations. During the LGM, a substantial decrease in sea level of around 120 m likely resulted in notable alterations to the pathways, strength, thermal structure, and heat transport capacity of the ITF.

Analysis of the TWT gradient (Table 3) of the S-N points from the surface to each thermocline depth (Table 3) during the LGM at the Makassar Strait, Molucca Sea, and Banda Sea indicates that temperatures are generally warmer at northern points compared to southern points within this depth range. The S-N TWT gradient at the Makassar Strait demonstrates clear seasonal variation from the surface to maximum thermocline depth of 254 m, where a robust negative TWT gradient is found in all seasons. In contrast, the Molucca Sea experiences a predominantly positive TWT gradient during DJF. While in Banda Sea, positive TWT gradients are mainly captured in three seasons, except SON. However, the temperature profile at Molucca Sea and Banda Sea remains with dominant warmer at the northern points and cooler at the southern points, extending from the surface to a depth of ~75-251 m in the Molucca Sea and ~45-186 m in the Banda Sea. The Banda Sea exhibits a unique thermal profile, maintaining a balanced range of cooler and warmer temperatures from the surface to a depth of 236 m during specific months. This suggests that the water transport from the tropical Pacific Ocean to the Makassar Strait via the Celebes Sea undergoes alterations *en route* due to differing water characteristics.

In the ITF's primary pathway, surface and intermediate fresher waters interact with the saltier Pacific tropical waters, leading to a gradual reduction in salinity maximum. The outflowing ITF water exhibits a fresher and cooler thermocline, along with an isohaline layer. The Celebes Sea maintains high salinity characteristics; however, its subsurface salinity maximum decreases southward along the Makassar Strait, ultimately vanishing prior to reaching the Banda Sea. The subsurface temperature

is lower, and the thermocline is notably shallower in the southern Makassar Strait relative to the northern region (Table 2).

A comparison of surface and thermocline temperatures among these three locations facilitates an evaluation of paleo-ITF variability between the PI and the LGM. All three records indicate a larger south-north TWT gradient during two key periods—the PI and the LGM—suggesting that the southern Makassar Strait, Molucca Sea, and Banda Sea were relatively fresher (indicated by the negative S-N TWT gradient) in the thermocline layer during these times, seasonally (Figures 4-5, Table 3), except in Molucca Sea and Banda Sea in DJF during LGM, in Banda Sea in MAM during LGM and PI, in Banda Sea in JJA during PI. This negative S-N TWT gradient implies a primarily weakened ITF during both LGM and PI. Fan et al. (2018) suggested that the diminished ITF strength during LGM, attributed to decreased sea levels, likely led to weakened thermal advection, resulting in cooler temperatures in the southern region compared to the relatively warmer northern region. During the PI, a reduced TWT gradient indicates a more robust ITF, facilitating the mixing and transport of warmer waters from the Pacific through Makassar Strait and Molucca Sea, which then circulates the waters to Banda Sea. This procedure promoted a more consistent thermocline temperature throughout the strait. Additionally, it is posited that the tidal mixing intensity of the Indonesian Sea under LGM conditions was comparable to PI, and the explanation for the heightened contrast in thermocline across the Makassar Strait pertains to the intensity of the Makassar Strait Throughflow (MSTF). This intensity influences the extent of warmer and saltier thermocline water transported across the strait, thereby affecting the temperature and salinity gradients between the sediment cores located in the north-south orientation.

Furthermore, Fan et al*.,* (2018) determined that the Southeast monsoon contributed to oceanic upwelling, leading to vertical mixing that could produce a significantly cooler thermocline in the shoaled region. Likewise, this condition aligns with the observation that a weakened ITF consistently coincides with a strengthened Mindanao Current during a contemporary El Niño-like state. A stronger Mindanao Current may facilitate the eastward movement of warm, saline water from the North Pacific into the Pacific North Equatorial Counter current, resulting in a reduced flow of warm water westward into the ITF. The increased eastward transport of warm water in an El Niño-like state may further facilitate the eastward propagation of the equatorial Pacific atmospheric convection center during the LGM.

The TWT gradients in the Molucca Sea and Banda Sea have not been examined in prior research. Only a study on TWT at the ITF's exit of Timor Sea was explored and indicated that the ITF's passage through the Timor Sea likely weakened during the LGM due to shallower water depths in that region at that time (Xu et al., 2008; Holbourn et al., 2011). During the LGM in the Molucca Sea, a steeper TWT gradient was observed in months of JJA, suggesting limited inflow of the ITF. Cooler thermocline waters remained in the southern Molucca Sea as a result of diminished warm water transport (Figure 4 and Table 3).

The results from the S-N TWT gradient at Banda Sea during LGM (Figure 4c) align with either Ding et al., 2013, who proposed a strengthened ITF during DJF and MAM seasons (indicate by negative TWT gradient), or Xu et al., 2008 and Holbourn et al*.,* (2011), who suggested a weakened ITF during the LGM in the Timor Sea; in the rest of the seasons in Banda Sea. This variation may result from the Banda Sea functioning as a significant outflow area for the ITF, where the thermocline depth and temperature reflect the final adjustments of ITF waters prior to their entry into the Indian Ocean. During the PI, a distinct warmer thermocline temperature is observed at the northern point in DJF and SON seasons, while a cooler thermocline temperature is noted at the southern point, in contrast to the thermocline temperature recorded during the LGM, particularly in DJF.

The analysis of the TWT gradient at the three locations—Makassar Strait, Molucca Sea, and Banda Sea—during the LGM indicates that the ITF is more pronounced and stronger to the east (Banda Sea) of Indonesian waters compared to the other stations (Makassar Strait and Molucca Sea) and compared to PI in all seasons (indicate by the positive and larger TWT gradient). This variation may correlate with the intensity of seasonal local winds and mixing processes.

# CONCLUSSIONS

This research examines the seasonal temperature distribution along specific ITF pathways in the Makassar Strait, Molucca Sea, and Banda Sea. The temperature distribution is examined in relation to the south (S) and north (N) thermocline water

temperature gradient to elucidate the strength of the ITF during the LGM in comparison to the present/PI. The depth of the thermocline layer during the LGM and the PI period appears comparable, yet it exhibits seasonal variability across southern and northern points. At Station 1, the thermocline depth during LGM ranges from 49 to 218 m in the south and 51 to 254 m in the north. At Station 2, it ranges from 55 to 250 m across the southern and northern points, while at Station 3, it spans from 48 to 238 m in the south and 48 to 218 m in the north. All three records indicate a larger south-north TWT gradient during the LGM—suggesting that the southern Makassar Strait, Molucca Sea, and Banda Sea were predominantly fresher compared to the northern part in thermocline layers during this time. The examination of the south-north TWT gradient across the Makassar Strait and Molucca Sea indicates a notable reduction in the ITF during the LGM, although this trend is not observed in the Banda Sea. The analysis of the TWT gradient at the Makassar Strait, Molucca Sea, and Banda Sea indicates that the ITF was stronger to the east (Banda Sea) of Indonesian waters relative to Makassar Strait and Molucca Sea during the LGM and compared to PI in all seasons. It has been suggested to be associated with decreased sea levels, leading to weakened thermal advection, resulting in cooler temperatures in the southern region compared to the relatively warmer northern region during the LGM. Moreover, this variation may relate to the intensity of seasonal local winds, mixing processes, and the remote influences of El Niño-like events, which could impact water transport along the pathway of the ITF. Further investigation is required to calculate ITF transport between the S-N stations vertically at each location.

## ACKNOWLEDGEMENTS

Investigation on TWT in this recent study is carried out by using model output of Community Climate System Model, version 4. Data was manageably taken from the World Data Center for Climate (WDCC). The WDCC is hosted by the German Climate Computing Center (Deutsches Klimarechenzentrum - DKRZ) in Hamburg and it was openly accessed from https://www.wdc-climate.de/ui/. Moreover, this study was supported by funding from Kemenristek/BRIN under PROGRAM RISET DASAR KEMITRAAN year 2021, scheme WORLD CLASS RESEARCH (WCR), contract number 588a/IT1.C01/TA.00/2021 and Program Penelitian dan Pengabdian kepada Masyarakat ITB (PPMI-ITB) year 2019.

## REFERENCES

Bradley, R.S., 1999. *Paleoclimatology: Reconstructing Climates of the Quaternary*. 2nd Edition, Academic Press, San Diego, 10p.

Brady, E.C., Otto-Bliesner, B.L., Kay, J.E., Rosenbloom, N., 2013. Sensitivity to Glacial Forcing in the CCSM4. *American Meteorological Society*, 26(6):1901-1925. https://doi.org/10.1175/JCLI-D-11-00416.1.

Brady, E.C., Stevenson, S., Bailey, D., Liu, Z., Noone, D., Nusbaumer, J., Otto-Bliesner, B. L., Tabor, C., Tomas, R., Wong, T., Zhang, J., Zhu, J., 2019. The Connected Isotopic Water Cycle in the Community Earth System Model version 1. *Journal of Advances in Modeling Earth Systems*, 11:2547–2566. https://doi.org/10.1029/2019MS001663.

Briegleb, B.P., and Light, B., 2007. A Delta-Eddington Multiple Scattering Parameterization for Solar Radiation in the Sea Ice Component of the Community Climate System Model. *University Corporation for Atmospheric Research*, *NCAR Technical Note* 4721STR, 100 pp.

Danabasoglu, G., Bates, S.C., Briegleb, B.P., Jayne, S.R., Jochum, M., Large, W.G., Peacock, S., and Yeager, S.G., 2012a. The CCSM4 ocean component. *Journal of Climate*, 25:1361–1389. https://doi.org/10.1175/JCLI-D-11-00091.1.

Danabasoglu, G., Yeager, S.G., Kwon, Y.O., Tribbia, J.J., Phillips, A., and Hurrell, J.W., 2012b. Variability of the Atlantic Meridional Overturning Circulation in CCSM4. *Journal of Climate*, 25:5153–5172. https://doi.org/10.1175/JCLI-D-11-00463.1.

Deser, C., Phillips, A., Tomas, R., Okumura, Y., Alexander, M., Capotondi, A., Scott, J., Kwon, Y.O., Ohba, M., 2012. ENSO and Pacific Decadal Variability in the Community Climate System Model Version 4. *Journal of Climate*, 25:2622–2651.

Ding, X., Bassinot, F., and Guichard, F., fang, N.Q., 2013. Indonesian Throughflow and monsoon activity records in the Timor Sea since the last glacial maximum. *Marine Micropaleontology*, 101:115 – 126.

Fan, W., Jian, Z., Chu, Z., Dang, H., Wang, Y., Bassinot, F., Han, X., Bian, Y., 2018. Variability of the Indonesian Throughflow in the Makassar Strait over the Last 30 ka. *Scientific Reports*, 8:5678. https://doi.org/10.1038/s41598–018–24055–1.

Feng, M., Zhang, N., Liu, Q., Wijffels, S., 2018. The Indonesian throughflow, its variability and centennial change. Geoscience Letters 5, 3. https://doi.org/10.1186/s40562-018-0102-2.

Gent, P.R., Danabasoglu, G., Donner, L.J., Holland, M.M., Hunke, E.C., Jayne, S.R., Lawrence, D.M., Neale, R.B., Rasch, P.J., Vertenstein, M., Worley, P.H., Yang, Z.-L., Zhang, M., 2011. The Community Climate System Model Version 4. *Journal of Climate*, 24:4973–4991. doi:10.1175/2011JCLI4083.1.

Gordon, A. L., 2005. Oceanography of the Indonesian Seas and Their Throughflow. *Oceanography*, 18(4):14-27.

Gordon, A. L., Sprintall, J., Van Aken, H. M., Susanto, D., Wijffels, S., Molcard, R., Wirasantosa, S., 2010. The Indonesian Throughflow during 2004–2006 as observed by the INSTANT program. *Dynamics of Atmospheres and Oceans*, 50(2):115–128. https://doi.org/10.1016/j.dynatmoce.2009.12.

Hendrizan, M., Kuhnt, W., and Holbourn, A., 2017. Variability of Indonesian Throughflow and Borneo Runoff During the Last 14 kyr. *Paleoceanography*, 32:1054–1069. https://doi.org/10.1002/2016PA003030.

Holbourn, A., Kuhnt, W., Xu, J., 2011. Indonesian Throughflow variability during the last 140 ka: the Timor Sea outflow. *Geological Society of London Special Publications*, 355:283–303. https://doi.org/10.1144/SP355.14.

Holland, M. M., Bailey, D. A., Briegleb, B. P., Light, B., and Hunke, E., 2012. Improved Sea Ice Shortwave Radiation Physics in CCSM4: The Impact of Melt Ponds and Aerosols on Arctic Sea Ice. *Journal of Climate*, 25:1413–1430.

Hu, S., Zhang, Y., Feng, M., Du, Y., Sprintall, J., Wang, F., Hu, D., Xie, Q., Chai, F., 2019. Interannual to Decadal Variability of Upper–Ocean Salinity in the Southern Indian Ocean and the Role of the Indonesian Throughflow. *Journal of Climate*, 32: 6403–6421. https://doi.org/10.1175/JCLI–D–19–0056.1.

Hunke, E. C., and Lipscomb, W. H., 2010. *CICE: The Los Alamos Sea Ice Model Documentation and Software User's Manual, Version 4.1.* Los Alamos National Laboratory. Tech. Rep. LA- CC-06-012, 76 pp.

Kageyama, M., Harrison, S. P., Kapsch, M.-L., Lofverstrom, M., Lora, J. M., Mikolajewicz, U., Sherriff-Tadano, S., Vadsaria, T., Abe-Ouchi, A., Bouttes, N., Chandan, D., Gregoire, L. J., Ivanovic, R. F., Izumi, K., LeGrande, A. N., Lhardy, F., Lohmann, G., Morozova, P. A., Ohgaito, R., Paul, A., Peltier, W. R., Poulsen, C. J., Quiquet, A., Roche, D. M., Shi, X., Tierney, J. E., Valdes, P. J., Volodin, E., and Zhu, J., 2021. The PMIP4 Last Glacial Maximum experiments: preliminary results and comparison with the PMIP3 simulations. *Climate of the Past*, 17(3):1065–1089.

Landrum, L., Holland, M.M., Schneider, D.P., and Hunke, E., 2012. Antarctic Sea Ice Climatology, Variability, and Late Twentieth-Century Change in CCSM4. *Journal of Climate*, 25:4817–4838. https://doi.org/10.1175/JCLI-D-11-00289.1.

Lauritzen, P. H., Mirin, A.A., Truesdale, J., Raeder, K., Anderson, J.L., Bacmeister, J., and Niele, R., 2012. Implementation of new diffusion/filtering operators in the CAM-FV dynamical core. *International Journal of High Performance Computing Applications,* 26:63–77.

Lawrence, P. J., and Chase, T. N., 2007. Representing a new MODIS consistent land surface in the Community Land Model (CLM3.0). *Journal Geophysical Research,* 112:G01023. https://doi.org/10.1029/2006JG000168.

Lee, S.K., Park, W., Baringer, M.O., Gordon, A.L., Huber, B., Liu, Y., 2015. Pacific origin of the abrupt increase in Indian Ocean heat content during the warming hiatus. *Nature Geoscience*, 8:445–449. https://doi.org/10.1038/ngeo2438.

Linsley, B.K., Rosenthal, Y., Oppo, D.W., 2010. Holocene evolution of the Indonesian Throughflow and the Western Pacific Warm Pool. *Nature Geoscience*, 3:578–583.

Meehl, G. A., and Coauthors, 2012. Climate System Response to External Forcings and Climate

Change Projections in CCSM4. *Journal of Climate*, 25:3661–3683.

Neale, R. B., Richter, J. H., and Jochum, M., 2008. The Impact of Convection on ENSO: From a Delayed Oscillator to a Series of Events. *Journal of Climate*, 21:5904–5924.

Pang, X., Bassinot, F., Sepulcre, S., 2021. Indonesian Throughflow variability over the last two glacial–interglacial cycles: Evidence from the eastern Indian Ocean. *Quaternary Science Reviews*, 256. https://doi.org/10.1016/j.quascirev.2021.106839.

Peltier, W. R. and Fairbanks, R. G., 2006. Global glacial ice volume and Last Glacial Maximum duration from an extended Barbados sea level record. *Quaternary Science Reviews*, 25:3322–3337. https://doi.org/10.1016/j.quascirev.2006.04.010.

Rachmayani, R., Prange, M., Schulz, M., dan Ningsih, S. N., 2019. Climate Variability in Indonesia from 615 Ka to Present: First Insights from Low-Resolution Coupled Model Simulations. *Die Erde*, 150(4). https://doi.org/10.12854/erde-2019-428.

Richter, J. H., and Rasch, P. J., 2008. Effects of Convective Momentum Transport on the Atmospheric Circulation in the Community Atmosphere Model, version 3. *Journal of Climate*, 21:1487–1499.

Shen, C., Moore, J.C., Kuswanto, H., Zhao, L., 2023. The Indonesian Throughflow circulation under solar geoengineering. *Earth Dynamics System*, 14(6):1317–1332. https://doi.org/10.5194/esd-14-1317-2023.

Smith, R. D., and Coauthors, 2010. *The Parallel Ocean Program (POP) reference manual*. Los Alamos National Laboratory Tech. Rep. LAUR-10-01853, 140 pp.

Sprintall, J., Wijffels, S.E., Molcard, R., Jaya, I., 2009. Direct estimates of the Indonesian throughflow entering the Indian Ocean: 2004–2006. *Journal Geophysical Research*, 114:C07001. https://doi.org/10.1029/2008JC005257.

Talley, L., 2013. Closure of the Global Overturning Circulation Through the Indian, Pacific, and Southern Oceans: Schematics and Transports. *Oceanography*, 26:80–97. https://doi.org/10.5670/oceanog.2013.07.

Thornton, P., et al., 2007. Vulnerability, climate change and livestock: Research opportunities and challenges for poverty alleviation. *SAT eJournal*, 4:1-23. www.icrisat.org/journal/SpecialProject/sp7.pdf.

Xu, J., Holbourn, A., Kuhnt, W., Jian, Z., Kawamura, H., 2008. Changes in the thermocline structure of the Indonesian outflow during Terminations I and II. *Earth Planet Science Letter*, 273:152–162. https://doi.org/10.1016/j.epsl.2008.06.029.

Zhang, P., Xu, J., Holbourn, A., Kuhnt, W., Pei, R., Xiong, Z., Li, Ti., 2024. Precession-Driven Variations in the Indonesian Throughflow Thermocline and Its Implications on the Agulhas Leakage. *Geophysical Research Letters*, 51. https://doi.org/10.1029/2024GL110520.